A&A 589, A38 (2016)
DOI: 10.1051/0004-6361/201527861

Astronomy & Astrophysics

Explosion of white dwarfs harboring hybrid CONe cores

E. Bravo[1], P. Gil-Pons[2], J. L. Gutiérrez[2], and C. L. Doherty[3]

[1] Escola Tècnica Superior d'Arquitectura del Vallès, Univ. Politècnica de Catalunya, Carrer Pere Serra 1-15, 08173 Sant Cugat del Vallès, Spain
e-mail: eduardo.bravo@upc.edu
[2] Departament de Física, Univ. Politècnica de Catalunya, 08034 Castelldefels, Spain
e-mail: pilar@fa.upc.edu,jordi.gutierrez@upc.edu
[3] Monash Centre for Astrophysics (MoCA), School of Physics and Astronomy, Monash University, 3800 Victoria, Australia

Received 30 November 2015 / Accepted 28 February 2016

ABSTRACT

Recently, it has been found that off-center carbon burning in a subset of intermediate-mass stars does not propagate all the way to the center, resulting in a class of hybrid CONe cores. The implications of a significant presence of carbon in the resulting massive degenerate cores have not been thoroughly explored so far. Here, we consider the possibility that stars hosting these hybrid CONe cores might belong to a close binary system and, eventually, become white dwarfs accreting from a nondegenerate companion at rates leading to a supernova explosion. We computed the hydrodynamical phase of the explosion of Chandrasekhar-mass white dwarfs harboring hybrid cores, assuming that the explosion starts at the center; this explosion occurs either as a detonation, as may be expected in some degenerate merging scenarios, or as a deflagration that afterward transitions into a delayed detonation. We assume these hybrid cores are made of a central CO volume, of mass $M_{\rm CO}$, surrounded by an ONe shell. We show that, in the case of a pure detonation, a medium-sized carbon-rich region, $M_{\rm CO}$ (<0.4 $M_{\odot}$), results in the ejection of a small fraction of the mantle while leaving a massive bound remnant. Part of this remnant is made of the products of the detonation, that is, Fe-group nuclei, but they are buried in its inner regions unless convection is activated during the ensuing cooling and shrinking phase of the remnant. In contrast, and somehow paradoxically, delayed detonations do not leave remnants other than for the minimum $M_{\rm CO}$ we explored of $M_{\rm CO}$ = 0.2 $M_{\odot}$, and even in this case the remnant is as small as 0.13 $M_{\odot}$. The ejecta produced by these delayed detonations are characterized by slightly smaller masses of ^{56}Ni and substantially smaller kinetic energies than the ejecta obtained for a delayed detonation of a "normal" CO white dwarf. The optical emission expected from these explosions most likely do not match the observational properties of typical Type Ia supernovae, although they make interesting candidates for the subluminous class of SN2002cx-like or SNIax.

Key words. stars: evolution – supernovae: general – white dwarfs – nuclear reactions, nucleosynthesis, abundances – hydrodynamics

1. Introduction

Supernovae are the result of the explosive end point to the evolution of stars of a wide variety of masses. Most massive stars go through successive phases of hydrostatic burning until they form an iron core, at which point they cannot obtain more energy by means of nuclear processes. Their fate can be either a collapse of the whole structure to form a black hole, or a collapse of the central region followed by ejection of the envelope. In the last case, the diffusion of radiation through the ejected material allows it to shine in what is known as a core-collapse supernova (for recent reviews, see Woosley & Janka 2005; Janka et al. 2007; Janka et al. 2012; Burrows 2013). In contrast, stars of lower mass end as white dwarfs (WD), which are essentially dead stars with a composition and mass that is set during their earlier central burning stages, and AGB phase and associated pulsations. White dwarfs that are composed of carbon and oxygen (CO) and belong to a binary system may be reactivated by accretion of matter from the companion star and, under favorable conditions, can undergo a final nuclear phase in which they are partially burnt to Fe-group elements and then explode. The nucleosynthesis is rich in unstable isotopes that decay and feed the subsequent optical display known as thermonuclear, or Type Ia (SNIa), supernova (Parthasarathy et al. 2007; Howell 2011; Parrent et al. 2014). The precise path to WD ignition is not completely understood. In principle, two possibilities are considered: either both components are WDs, i.e., the double degenerate channel (DD), or only one of them is a WD, i.e., the single degenerate channel (SD).

There exists an initial mass frontier between core collapse and white dwarf formation. This frontier is located in the region of intermediate-mass stars (IMS), whose masses lie in the range ~7–11 $M_{\odot}$; these limits are strongly dependent on progenitor metallicity and input model physics (Woosley et al. 2002; Eldridge & Tout 2004; Smartt 2009; Ibeling & Heger 2013; Doherty et al. 2015). Stars in this mass range go through a final hydrostatic burning phase transmutating carbon into oxygen and neon (ONe; see Nomoto 1984; Ritossa et al. 1999; Siess 2010). Unlike CO WDs, WDs made of ONe that belong to a binary system collapse, rather than explode, when they accrete matter up to the Chandrasekhar mass; this is why they are usually excluded from the set of putative progenitors of SNIa (Miyaji et al. 1980; Nomoto 1984; Nomoto 1987; Gutiérrez et al. 1996; Gutiérrez et al. 2005). Furthermore, merging of two WDs made of CO in a DD scenario may lead to non-explosive C-burning and mutation of the composition into ONe, with the same result as in single Chandrasekhar-mass WDs made of ONe of collapsing to a neutron star rather than exploding (Saio & Nomoto 1998). Current multidimensional simulations of the merging of WDs nurture the hope of avoiding this collapse (e.g., Pakmor et al. 2010; Moll et al. 2014; Raskin et al. 2014).

However, these results are preliminary because of the extremely difficult numerical problems posed by ignition in the outer shells of the star, which are usually affected by low spatial resolution in two or three dimensions.

In this context, it is interesting to recall that very efficient neutrino cooling at the innermost stellar regions causes C-burning to start off-center (see Dominguez et al. 1993; Garcia-Berro & Iben 1994) except in the most massive cases of the IMS mass-range. Eventually C-burning extends further in the core, but at a certain point the physical conditions required for the burning front to propagate are not met and the process stops, leaving a CO central region with a few tenths of $M_{\odot}$ surrounded by an ONe shell. Recent analysis (Denissenkov et al. 2013) has shown that such a stratified chemical structure of the core might occur because of the effect of convective boundary mixing, which is able to prevent the C-burning flame from reaching the central regions of the star. In fact, similar structures that are composed of a central carbon-rich region surrounded by an ONe (i.e., carbon-poor) zone have been found using different evolutionary codes, such as MONSTAR (Doherty et al. 2010) or the code used by Garcia-Berro & Iben (1994). The question is nevertheless far from closed (see, e.g., Waldman & Barkat 2007), and it is interesting to analyze the outcome of different configurations of such CONe cores.

The existence of hybrid CONe WD warrants a reevaluation of the final outcome of the evolution of IMS. The presence of carbon at the center of the WD makes the explosion rather than collapse to a neutron star feasible again, and the question is whether the explosion of such a carbon-rich core surrounded by a large carbon-depleted ONe mantle would look similar to a SNIa.

The size of the initial mass range of IMS that are able to end as a hybrid CONe WD is ∼0.1–0.2 $M_{\odot}$ in standard calculations (e.g., Doherty et al. 2010; Ventura & D'Antona 2011; Doherty et al. 2015), but it can be as large as ∼0.4–1.0 $M_{\odot}$, depending on the strength of convective boundary mixing (Denissenkov et al. 2013) and uncertainties in C-burning rates (Chen et al. 2014). We note that CONe cores are found over a large variety of metallicities (Doherty et al. 2015) and also for a range of helium enrichments (Shingles et al. 2015). In any case, a narrow mass range would allow us to explain at most a few percent of the observed SNIa (Meng & Podsiadlowski 2014). In particular, it has been advocated that their explosion might match some class of peculiar SNIa (Chen et al. 2014; Meng & Podsiadlowski 2014), and that the narrow initial mass range would favor the homogeneity of the observational properties within that class.

Currently, three, more or less homogeneous, classes of subluminous thermonuclear supernovae have been identified: the so-called SNIax, the .Ia, and the Ca rich. The best studied is the SNIax group (Li et al. 2003; Foley et al. 2013; Stritzinger et al. 2015; White et al. 2015), which is characterized by maximum-luminosity velocities 2000–8000 km s^{-1} slower and luminosities 0.5–5 mag dimmer than normal SNIa. Their photosphere is hotter at maximum luminosity than that of normal SNIa. This group follows a different trend in the light-curve peak brightness vs. width plane, although not far from normal SNIa. They have been tentatively identified with failed deflagrations of massive WDs leaving a bound remnant. As yet, no Iax supernova has been found in an elliptical galaxy (but SN 2008ge exploded in an S0 galaxy), thus suggesting that their progenitors belong to a young population; the galaxies hosting all known Iax supernovae have active regions of star formation, except for the mentioned case of SN 2008ge. The mass range for stars forming CONe cores is consistent with such environments of Iax supernovae. This possibility is further supported by the observed colors of the putative progenitors of SN 2008ha and SN 2012Z, which are consistent with those of evolved intermediate-mass stars (McCully et al. 2014a; Foley et al. 2014). The .Ia class (Kasliwal et al. 2010; Drout et al. 2013) designation is suggestive of a SNIa with all its relevant magnitudes scaled down by an order of magnitude; this class is characterized by a very fast evolution of the light curve, whose peak is about 3 mag dimmer than normal SNIa (i.e., .Ia are about an order of magnitude less brilliant), and an ejected mass of ^{56}Ni of order 0.02–0.03 $M_{\odot}$. Their characteristic velocity, however, is of the same order as normal SNIa, which suggests that the ejecta mass is small, at about a tenth of a Chandrasekhar mass. Drout et al. (2013) find that the ejecta of SN2005ek, a .Ia candidate, are dominated by oxygen, while Kasliwal et al. (2010) speculate that the progenitor of SN2010X might be an ONeMg WD. Finally, the Ca-rich class (Perets et al. 2010; Kasliwal et al. 2012; Valenti et al. 2014) is defined by an unusually large content of calcium, which can amount to as much as half of the ejecta mass. However, at present, their thermonuclear origin has not been robustly established.

Here, we are concerned with the outcome of the explosion of hybrid WDs. How their drastic chemical differentiation influences the hydrodynamic behavior of the explosion, and what is the range of properties of their ejecta. We do not calculate the optical outcomes of the explosions, but concentrate on identifying the most interesting combinations of progenitor system and explosion type. We start by considering the formation of a hybrid CONe WD as a result of the evolution of the primary star, an IMS, in a close-binary system. Next, we succinctly explain the methods used in our study and the characteristics of the initial models. After that, we provide the results of the simulations of the explosions of hybrid CONe WDs, discuss the results in context of the properties of the aforementioned subgroups of peculiar SNIa, and provide our conclusions.

2. Formation of hybrid CONe WDs

The formation of a hybrid CONe degenerate core is a consequence of incomplete core C-burning. We consider here two classes of hybrid CONe WDs, characterized by very different sizes and masses of the CO central region. The first class, which we call large hybrid cores (LHC), is obtained following standard evolutionary calculations of IMS within a narrow mass range (Doherty et al. 2010; Ventura & D'Antona 2011), and harbor a large CO central volume surrounded by a thin ONe layer. They are the result of carbon burning starting very far off-center in IMS with core masses of ∼1.04–1.06 $M_{\odot}$, and switching off before reaching the center because of cooling by neutrinos at the innermost region of the core. In the cases that concern us, i.e., the lightest objects able to ignite carbon, suitable conditions for carbon burning are not recovered after the first off-center burning episode (for instance, Ritossa et al. 1999; Gil-Pons & García-Berro 2001; Siess 2006; Doherty et al. 2010).

The second class, which we call medium-sized hybrid cores (MSHC), is the result of IMS evolution when either modified recipes for the strength of convective boundary mixing or uncertainties in the C-burning rates are allowed (Denissenkov et al. 2013; Chen et al. 2014). The mass of the carbon-rich central volume is $M_{\rm CO} \sim 0.2{-}0.45\ M_{\odot}$, surrounded by an ONe layer that is thicker than that in the LHC class. In this class, the quench of the C-burning flame is a result of the decoupling between the fuel –^{12}C– profile and the thermal profile, due

to efficient convective boundary mixing (see Denissenkov et al. 2013). As the flame advances inward, the carbon abundance this flame faces decreases steadily because of the convective mixing of fuel with ashes until, finally, it is so small that carbon ignition is no longer possible and a carbon-rich central volume remains unburnt (for a recent critical reevaluation of the role of convective overshooting, see Farmer et al. 2015). In all cases there remains a small residual abundance of ^{12}C in the ONe region, a feature that is in fact common to all super-AGB star cores.

To become a thermonuclear supernova, this model has to belong to a close binary whose orbital parameters must meet two requirements. First, the initial orbital period must be such that the Roche-lobe overflow from the primary and, therefore, a mass transfer episode would not occur until it has become a giant hosting a deep convective envelope. Second, the initial mass ratio of the two components, $q = M_1/M_2$, must be relatively low, for example, below 1.5–2, so that merger episodes can be avoided. Both conditions determine initial orbital distances of a few hundred solar radii and secondary masses M_2 above ≈3–4 $M_\odot$. Such systems start interacting once the primary component reaches red giant dimensions, and go through a first common envelope (CE) episode, after which the primary is a He-burning core and the secondary remains as main sequence star. A second giant (super-AGB) phase of the primary leads to a new mass transfer episode that is also accompanied by the occurrence of a CE, after which the primary becomes an almost bare hybrid CONe degenerate core and the secondary is still a main sequence star. The size of the carbon-rich region within the hybrid CONe core depends on the location of the carbon flame at the onset of the second mass transfer episode, in addition to other evolutionary ingredients mentioned above.

Depending on the details of the evolution of orbital parameters, which are beyond the scope of this work, different options ensue at this point. If the orbital shrinkage has been significant, gravitational wave radiation might induce further shrinkage and allow Roche-lobe overflow of the secondary component while it is still a main sequence star. Otherwise, reverse mass transfer can occur when the secondary reaches a subgiant or giant phase. In either case, if the final outcome is to be a thermonuclear supernova, instead of a nova, mass accretion rates onto the white dwarf must be above 10^{-7} $M_\odot$/yr (Nomoto et al. 2007).

3. Models and methods

We calculated the explosion of both LHC and MSHC Chandrasekhar-mass WDs[1] with a version of the one-dimensional code described in Bravo & Martínez-Pinedo (2012), upgraded to include a more accurate treatment of the coupling between hydrodynamics and nuclear reactions (Bravo et al., in prep.). The hydrocode implements a nuclear network of up to 722 nuclides, from free neutrons to ^{101}In (see Table 1 in Bravo & Martínez-Pinedo 2012). The nuclear network is solved simultaneously with the hydrodynamic equations and it is adaptive, i.e., its size and membership are decided at each time step and at each mass shell according to a set of rules depending on the abundances and reaction rates.

The initial model fed to the hydrodynamics code was a WD with central density 2.6×10^9 g cm^{-3} and total mass $M_{\rm WD}$ = 1.37 $M_\odot$, in hydrostatic equilibrium. Two flavors of the explosion of Chandrasekhar-mass WDs were explored, either a direct detonation (DETO) starting at the center of the star or a delayed detonation (DDT) that starts at the center as a subsonic flame, propagates at a small fraction of the sound velocity (3% in our models), and later makes a transition to a detonation at a prescribed density, $\rho_{\rm DDT}$. The thermal structure of the WD was different for both explosion mechanisms. In the DDT models, we started from an isothermal WD at $T = 10^7$ K. On the other hand, the initial WD was adiabatic in the DETO models with a central temperature of $T_{\rm c} = 10^9$ K. Further details of the implementation of the explosion mechanisms in the hydrocode can be found in the Appendix of Badenes et al. (2003).

In a recent work, Kromer et al. (2015) perform a three-dimensional simulation of a pure deflagration of the carbon-rich core of a hybrid CONe WD, assuming that the flame cannot propagate into the ONe mantle. The present models complement the models of Kromer et al. with respect to the explosion mechanism. We compare results in Sect. 4.3.4.

The chemical composition of the WD and its imprint on the explosion outcome is the main point of interest of this work. To have a realistic basis on which to explore different combinations of hybrid core masses, mantle masses, and mass fraction of the main species, we followed the hydrostatic evolution of an IMS star with the aid of MONSTAR (see, e.g., Frost & Lattanzio 1996; Campbell & Lattanzio 2008, and references therein) in the version described in Gil-Pons et al. (2013). The star had a ZAMS mass 8.25 $M_\odot$[2] and solar metallicity, Z = 0.02 (Grevesse & Noels 1993), and we followed its evolution up to the first few thermal pulses during its AGB phase. In Fig. 1 (top panel), we show the composition profiles at the end of our hydrostatic calculation. The degenerate core has a mass of ∼1.04 $M_\odot$ with a structured chemical profile made of a carbon-rich, $X(^{12}{\rm C}) \approx 0.315$, central volume with $M_{\rm CO} \sim$ 0.74 $M_\odot$, a thin C-burning front, and a neon-rich mantle. The transition between the carbon-rich central volume and carbon-poor mantle is abrupt; this property is shared with the hybrid cores obtained by Denissenkov et al. (2013). In the outermost regions of this core thin helium and hydrogen burning fronts can be identified. The whole structure is surrounded by a massive, but tenuous hydrogen-rich envelope. In a binary scenario relevant for the case we consider, a first mass-loss episode causes the loss of most of the H-rich envelope and a second mass-loss episode removes most of the He-rich remnant envelope. As shown in Gil-Pons et al. (2003), the He and C-burning processes and the resulting core compositions are not altered by such mass transfer, except that the expected progenitor mass corresponds to 0.5 $M_\odot$ more massive models. Therefore, for the present work, we can simply use single star evolution models.

In Table 1 we summarize the studied cases. For the MSHC, we considered carbon-rich regions of masses, $M_{\rm CO}$ = 0.2, 0.3, and 0.4 $M_\odot$ (models 1–19), while for the LHC we chose $M_{\rm CO}$ = 0.6, and 0.74 $M_\odot$ (models 20–23). In all cases, the carbon-rich region is composed of carbon, oxygen, and neon with mass fractions that are similar to the carbon-rich region in the hydrostatic

[1] The explosion of a Chandrasekhar-mass WD can be representative of the SD as well as the DD channel. In the first case, a hybrid-core WD accrets matter from a nondegenerate companion until carbon fusion runs away at or near the center. In the DD case, there are several possibilities; one of these is the merging of both WDs and the disruption of the less massive to form a corona or accretion disk around the most massive WD. Later, this structure is accreted by the primary at a pace that is slow enough that there is no ignition of carbon in its outer regions. In this situation, the evolution of the accreting WD ends in a similar form as described for the SD scenario.

[2] Owing to different convective boundary approaches used during the core He burning phase of evolution, we find hybrid CONe cores at initial masses ∼1.5 $M_\odot$ greater than those found in Denissenkov et al. (2013).

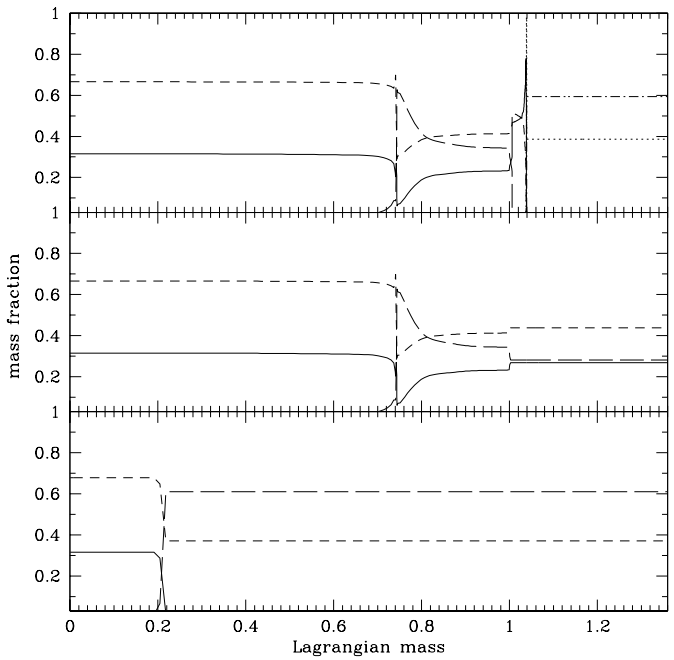

Fig. 1. Chemical profile of the AGB core at the beginning of the thermal pulses (*top*) and the pre-explosion WDs of models 22 and 23 (*middle*) and of models 1–6 (*bottom*); see Table 1. Solid line indicates C, short dashed line indicates O, long dashed line indicates Ne, dotted line indicates He, and dot-dashed line indicates H.

model shown in Fig. 1, i.e., $X(^{12}\mathrm{C}) = 0.315$, $X(^{16}\mathrm{O}) = 0.678$, and $X(^{20}\mathrm{Ne}) = 0.007$, and surrounded by a carbon-depleted mantle.

LHC models 22 and 23 mapped the chemical structure shown in Fig. 1 precisely up to 1.0 $M_\odot$, to avoid the H and He burning regions, and then added mass shells up to $M_{\rm WD}$ with the same chemical composition as in the shell at Lagrangian mass 1.0 $M_\odot$ (middle panel in Fig. 1).

In all the other cases (models 1–21), we simplified the chemical structure of the mantle as follows. By default, and with the aim of introducing as few free parameters as possible in the explosion models, we assume a homogeneous mantle composed of oxygen and neon up to $M_{\rm WD}$ (for an example, see the bottom panel in Fig. 1). We adopted different prescriptions for the abundance of oxygen in the mantle to check its impact on the results. In most models, we assumed a mass fraction of ^{20}Ne in the mantle equal to the maximum mass fraction found in Fig. 1 (top panel), $X_{\rm out}(^{20}\mathrm{Ne}) = 0.63$, which belongs to a mass coordinate of ~0.74 $M_\odot$, and the corresponding ^{16}O mass fraction, $X_{\rm out}(^{16}\mathrm{O}) = 0.37$. Since this choice is somewhat arbitrary, we also explored models with different compositions of the mantle, i.e., more reactive than in the default case, either by adding a few percent ^{12}C (models 2 and 8) or by increasing $X_{\rm out}(^{16}\mathrm{O})$ at the expense of $X_{\rm out}(^{20}\mathrm{Ne})$ (see column five in Table 1, and Sect. 4.3.1). Finally, we explored the presence of a mantle formed by two layers: an inner one with the default composition mentioned above, and an external one rich in carbon, $X_{\rm ext}(^{12}\mathrm{C}) = 0.32$, with a mass $M_{\rm ext}$ (column six). In Sect. 4.3.2 we show that the precise structure of the mantle has no impact on the outcome of the explosion of these models.

The initial models described above assume that the chemical differentiation established during the He-burning and quenched C-burning super-AGB phase is maintained up to the supernova explosion in the form of a hybrid core. However, in the last stages of evolution prior to thermal runaway of a Chandrasekhar-mass WD, the energy released by the incipient carbon fusion reactions is enough to drive convection (Piro & Bildsten 2008; Piro & Chang 2008)[3]. The convective core that develops is usually thought to encompass most of the WD, which in our case would destroy the chemically differentiated structure of the hybrid core. Nevertheless, there are uncertainties about the feasibility of such a huge convective core. First, in general, the eventual activation of URCA pairs might limit the reach of convective motions (Stein & Wheeler 2006; Podsiadlowski et al. 2008; Denissenkov et al. 2015) and preserve the original chemical structure. Second, specific to hybrid-core WDs, the presence of an abrupt separation between the carbon-rich central volume and the carbon-depleted mantle might allow for the operation of a self-regulating mechanism restricting the extent of convection. Convection during carbon simmering is regulated by the release of nuclear energy near the center of the WD. When convection reaches the ONe mantle and mixes this mantle with the material in the core, the carbon mass fraction in the center is expected to decrease (in addition to the effect of carbon consumption by nuclear reactions). As a result, the nuclear energy generation rate may decrease, which would affect the reach of convective motions. Through this mechanism, the carbon-depleted mantle may provide a natural frontier for the convective core, avoiding full mixing with the carbon-rich central volume. However, a proper determination of the extent of such an effect, even if it is relevant at all, would require following the evolution of the hybrid WD during the carbon simmering phase, which is beyond our scope.

In view of the above uncertainties, full mixing of the WD prior to explosion cannot be discarded. To explore its consequences, we calculated additional models of the explosion of homogeneous WDs representative of the full mixing of some of the hybrid-core WDs discussed before. (models 24–28 in Table 1). We address these homogeneous models in Sect. 4.3.3.

Finally, models 29–32 are reference delayed-detonation models with varying $\rho_{\rm DDT}$, in which the initial WD had a homogeneous composition, i.e., without a differentiated core, of $X(^{12}\mathrm{C}) = X(^{16}\mathrm{O}) \simeq 0.5$, with traces of heavier species with solar metallicity ratios. These models, which do not come from hybrid-core WDs, are identified in Table 1 with $M_{\rm CO} = 1.37\ M_\odot$. These kinds of models have been successfully compared to Type Ia supernovae and remnants in the past.

4. Results

The results of our supernova simulations are shown in Table 1 and in Fig. 2. We start by discussing the results of the simulations of our default configuration, i.e., a homogeneous mantle depleted of carbon and with an oxygen abundance of $X_{\rm out}(^{16}\mathrm{O}) = 0.37$. The dependence on several parameters of the initial model is discussed later.

4.1. Explosion of large hybrid core Chandrasekhar-mass WDs

The outcomes of the explosions of LHC models with $M_{\rm CO}$ of 0.6 and 0.74 $M_\odot$ are similar. The main difference between these models is derived from the lower nuclear binding energy of the composition of the WD with the smaller $M_{\rm CO}$. These explosions completely disrupt the WD leaving no bound remnant. Both DETO models (20 and 22) incinerate almost the whole WD and

[3] Another mechanism of chemical mixing would be gravitational settling, whose efficiency would depend on the time elapsed since the formation of the hybrid-core WD and the supernova event.

Table 1. Summary of results of the simulated explosions of hybrid-core CONe WDs.

ID	M_{CO} ($M_\odot$)	Burning mode[a]	$\rho_{DDT,7}$[b]	$X_{out}(^{16}O)$ ($M_\odot$)	M_{ext}	M_{rem} ($M_\odot$)	$M(^{56}Ni)$[c] ($M_\odot$)	M(IME) ($M_\odot$)	M(IGE) ($M_\odot$)	K[d] (foes)	Comment	
1	0.2	DETO	–	0.37	–	1.30	0	–	–		no optical display	MSHC
2	0.2	DETO	–	0.37[e]	–	1.30	0	–	–		no optical display	
3	0.2	DETO	–	0.37	0.57	1.28	0	0.002	–		no optical display	
4	0.2	DDT	1.1	0.37	–	0.12	0.08	0.021	0.095	0.06	slow ejecta	
5	0.2	DDT	1.4	0.37	–	0.13	0.07	0.023	0.072	0.05	slow ejecta	
6	0.2	DDT	1.4	0.37	0.57	0.014	0.10	0.085	0.18	0.09	slow ejecta	
7	0.3	DETO	–	0.37	–	1.00	0	–	–		no optical display	
8	0.3	DETO	–	0.37[e]	–	0.88	0	–	–		no optical display	
9	0.3	DETO	–	0.63	–	1.00	0	–	–		no optical display	
10	0.3	DDT	0.9	0.37	–	–	0.27	0.489	0.374	0.52	SNIax?	
11	0.3	DDT	1.1	0.37	–	–	0.35	0.490	0.461	0.63	SNIax?	
12	0.3	DDT	1.4	0.37	–	–	0.44	0.450	0.583	0.73	SNIax?	
13	0.3	DDT	1.7	0.37	–	–	0.54	0.395	0.681	0.80	SNIax?	
14	0.3	DDT	2.0	0.37	–	–	0.63	0.355	0.759	0.85	SNIax?	
15	0.4	DETO	–	0.37	–	–	0.10	$<10^{-3}$	0.414	0.09	slow ejecta	
16	0.4	DETO	–	0.63	–	–	0.95	0.004	1.36	1.28	almost no IME	
17	0.4	DETO	–	0.37	0.57	–	0.10	$<10^{-3}$	0.414	0.09	slow ejecta	
18	0.4	DETO	–	0.37	0.77	–	0.10	$<10^{-3}$	0.415	0.09	slow ejecta	
19	0.4	DDT	1.4	0.37	–	–	0.46	0.437	0.597	0.76	SNIax?	
20	0.6	DETO	–	0.37	–	–	0.95	0.004	1.36	1.30	almost no IME	LHC
21	0.6	DDT	1.4	0.37	–	–	0.52	0.386	0.649	0.82	SNIax?	
22	0.74	DETO	–	0.37	–	–	0.95	0.003	1.36	1.43	almost no IME	
23	0.74	DDT	1.4	0.37	–	–	0.59	0.451	0.710	1.09	SNIax?	
Models with mixed initial composition[f]												
24	0.2–0.4[g]	DETO	–		–	–	0.95	0.003	1.36	1.29	almost no IME	
25	0.2–0.4[g]	DDT	1.4		–	1.26	0	–	–		no optical display	
26	0.2–0.4[h]	DETO	–		–	–	0.95	0.002	1.36	1.37	almost no IME	
27	0.2–0.4[h]	DDT	1.4		–	–	0.59	0.427	0.712	0.99	SNIax?	
28	0.74[i]	DDT	1.4		–	–	0.61	0.443	0.726	1.11	SNIax?	
Reference models without a hybrid core												
29	1.37	DDT	1.1	0.5	–	–	0.54	0.491	0.697	1.29	normal SNIa	
30	1.37	DDT	1.4	0.5	–	–	0.66	0.409	0.818	1.35	normal SNIa	
31	1.37	DDT	1.7	0.5	–	–	0.74	0.347	0.904	1.40	normal SNIa	
32	1.37	DDT	2.0	0.5	–	–	0.79	0.299	0.964	1.42	normal SNIa	

Notes. [a] Burning mode: DETO = pure detonation; DDT = delayed detonation. [b] Density of deflagration-to-detonation transition in DDT models in 10^7 g cm^{-3}. [c] This column and the next two give the ejected mass of ^{56}Ni, intermediate-mass elements (IME), and iron-group elements (IGE), respectively. [d] Kinetic energy of the ejecta (1 foe = 10^{51} erg). [e] Initial abundance of $X(^{12}C)$ set to 0.02 outside M_{CO}. [f] WD born with hybrid core, but mixed during carbon simmering. [g] Model with $X(^{12}C) = 0.10$, representative of the result of the mixing between hybrid cores with M_{CO} within the range given in column two and a mantle with its default composition, $X_{out}(^{16}O) = 0.37$ and $X_{out}(^{20}Ne) = 0.63$. [h] Model with $X(^{12}C) = 0.20$, representative of the result of the mixing between hybrid cores with M_{CO} within the range given in column two and a mantle formed by two layers, an inner layer with the default composition and an external layer that is rich in carbon, $X_{ext}(^{12}C) = 0.32$, with a mass $M_{ext} = 0.57\ M_\odot$. [i] Initial composition obtained by full mixing of that of the initial model of ID 22 (and ID 23).

eject a huge mass of ^{56}Ni, but almost no intermediate-mass elements (IME). Since the clear detection of IME at maximum light is one of the defining properties of SNIa, these pure detonation models cannot match observations, just as with the detonation of homogeneous CO WDs.

On the other hand, DDT models (21 and 23) produce amounts of ^{56}Ni and IME that are in agreement with the predictions of normal SNIa models, but the kinetic energies of their ejecta are 0.82 and 1.09 foes, respectively. These kinetic energies are substantially smaller than those attributed to typical SNIa for their $M(^{56}Ni)$ (see, e.g., Mazzali et al. 2007; Woosley et al. 2007, and Fig. 2). In both DDT models, small masses of unburned ^{16}O, ~0.14 $M_\odot$, are ejected, while the masses of ^{12}C are negligible. The similarity of the results of $M_{CO} = 0.6$ and 0.74 $M_\odot$ shows that the composition of the mantle is not a relevant factor determining the outcome of the explosion of LHC models.

4.2. Explosion of medium-sized hybrid core Chandrasekhar-mass WDs

The result of the explosion of WDs with M_{CO} in the range 0.2–0.4 $M_\odot$ requires more explanation. Pure detonation models 1, 7, and 15, are characterized by a small release of nuclear binding energy. In all of these models, the detonation consumes the whole carbon-rich region, but is unable to propagate into the mantle due to the reduced flammability of oxygen as

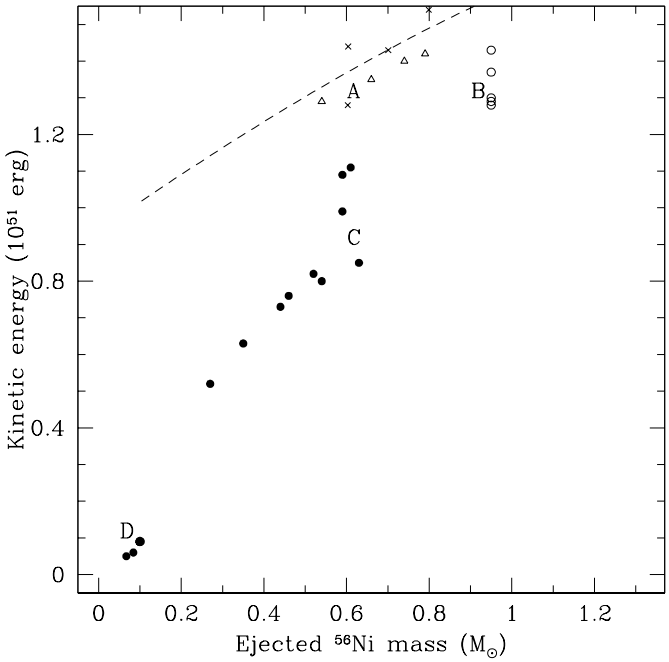

Fig. 2. Location of the computed explosions of hybrid CONe WDs in the K-$M(^{56}\mathrm{Ni})$ plane in context with standard SNIa models. Empty circles stand for pure detonations of hybrid WDs, while solid circles are for delayed detonations of the same objects. Empty triangles belong to delayed detonations of homogeneous CO WDs with varying ρ_{DDT}, which can account for normal SNIa (models 29–32 in Table 1). DETO models 15, 17, and 18 cannot be distinguished because their location coincides with that of DDT model 6. Crosses belong to the models of Ohlmann et al. (2014). The dashed line shows the approximate location of the normal SNIa models according to Mazzali et al. (2007), ranging from .08 $M_\odot$ of ^{56}Ni for the faint SN1991bg to .94 $M_\odot$ for the bright SN1994ae, and Woosley et al. (2007), who provide a range of kinetic energies. The four regions labeled with letters group models with more or less homogeneous characteristics (see text for further details).

compared to carbon. However, the result of the explosion depends sensitively on M_{CO} because we are considering masses close to the minimum incinerated mass necessary to unbind a Chandrasekhar-mass WD. The $M_{\mathrm{CO}} = 0.2\ M_\odot$ case releases an amount of nuclear energy that is too low, and the explosion leaves a large remnant of 1.30 $M_\odot$, i.e., only 0.07 $M_\odot$, composed of oxygen and neon, is ejected. The outcome of the detonation of the $M_{\mathrm{CO}} = 0.3\ M_\odot$ model is similar, with the only difference that the ejected mass is larger, and is still composed exclusively of oxygen and neon. No significant optical display, similar to any flavor of supernova, is expected from such objects. Nevertheless, the bound structures would be inflated and hot for some time, which would make them brighter than inert WDs of the same mass and potentially detectable at distances that are not too large.

The pure detonation model with $M_{\mathrm{CO}} = 0.4\ M_\odot$ is energetic enough to unbind the whole WD, even though just a very small fraction of the mantle is burnt. The final kinetic energy, 0.09 foes, as well the ejected mass of ^{56}Ni, 0.10 $M_\odot$, are very small.

The result of the DDT models varies qualitatively as a function of M_{CO} but, in all cases studied, more mass is burnt than in the corresponding DETO models. For $M_{\mathrm{CO}} = 0.2\ M_\odot$ (models 4 and 5), there remains a small bound remnant of ∼0.1 $M_\odot$, while the ejecta has a small kinetic energy, a few hundredths of 10^{51} erg, and small ^{56}Ni mass. These results are similar to those obtained for the pure detonation of the $M_{\mathrm{CO}} = 0.4\ M_\odot$ case, and do not depend significantly on the value of ρ_{DDT}.

The result of the delayed-detonation changes dramatically for $M_{\mathrm{CO}} > 0.2\ M_\odot$. Models 10–14 and 19 are similar to the DDT models of LHC, i.e., the WD is completely disrupted and the amount of ^{56}Ni ejected is within that expected for normal SNIa, while the kinetic energy is relatively small. There is a monotonic increase of both the mass of ^{56}Ni and the kinetic energy as a function of M_{CO} for a given ρ_{DDT}. For instance, at $\rho_{\mathrm{DDT}} = 1.4 \times 10^7$ g cm^{-3}, the range of ^{56}Ni masses covered by DDT models of both LHC and MSHC, leaving no bound remnant is 0.44–0.59 $M_\odot$ and the range of kinetic energies 0.73–1.09 foes. Allowing for different DDT transition densities, the amount of ^{56}Ni synthesized monotonically increases with ρ_{DDT}, which is similar to that found for the reference models 29–32. The kinetic energy, however, remains much smaller than in these reference models.

It is remarkable that, in all the MSHC models just discussed, pure detonation, which is the most violent burning mode, leads to explosions that are less energetic than the explosions due to delayed detonation. This apparent paradox can be understood as resulting from pure detonations entering the ONe mantle at high densities, combined with a monotonically decreasing nuclear energy release in detonations as a function of fuel density. Since pure detonations do not allow for any hydrodynamic response of the surrounding matter, the densities at which they arrive at the ONe mantle are the same as in the initial structure at carbon runaway, that is above 10^9 g cm^{-3} for $M_{\mathrm{CO}} = 0.2$–$0.4\ M_\odot$. Figure 3 shows the ratio of the nuclear energy released in a Chapman-Jouguet detonation to the increase in specific internal energy of the fuel within the shock front (just before nuclear reactions commence), as a function of fuel density. At fuel densities below ∼10^8 g cm^{-3}, with little dependence on the precise composition of the fuel, the energy released within the reaction layer of a detonation is enough to drive the fuel to the shocked state, where it starts burning and releasing energy that allows more fuel to detonate (Khokhlov 1988). In these conditions, the detonation can self-sustain once it has been initiated. In contrast, at higher densities, the final state of the detonation ashes is so hot that a substantial fraction of the produced iron-group elements (IGE) photodisintegrate and the final products are a mixture of IGE, IME, and light elements with the corresponding reduction in the nuclear energy yield. The nuclear energy invested in the creation of IME and light elements is restored later because of their recombination when matter expands and density decreases by about one order of magnitude or more, but this cannot occur while the detonation is alive because of its supersonic nature. Thus, the nuclear energy released at large densities is insufficient to shock the fuel to the desired state, and a piston or another source of energy external to the detonation itself would be needed[4] to sustain the burning wave. As a result, the pure detonation dies shortly after entering the ONe mantle.

In the DDT models, burning propagation is initially subsonic, as a deflagration, leaving time for matter to expand before arriving at the ONe mantle. The densities at which the detonation front arrives at the mantle, for example, in models 12 and 19, are of order 10^7 g cm^{-3}, which is low enough to allow self-sustainability of the burning front. The exception are the models with $M_{\mathrm{CO}} = 0.2\ M_\odot$, for example, model 5, in which

[4] Usually, such a piston-like effect is provided in pure detonation models by the supersonic burning of a region close to the center of the WD, as a result of a shallow thermal gradient, which gives a phase velocity of the combustion front above the sound speed.

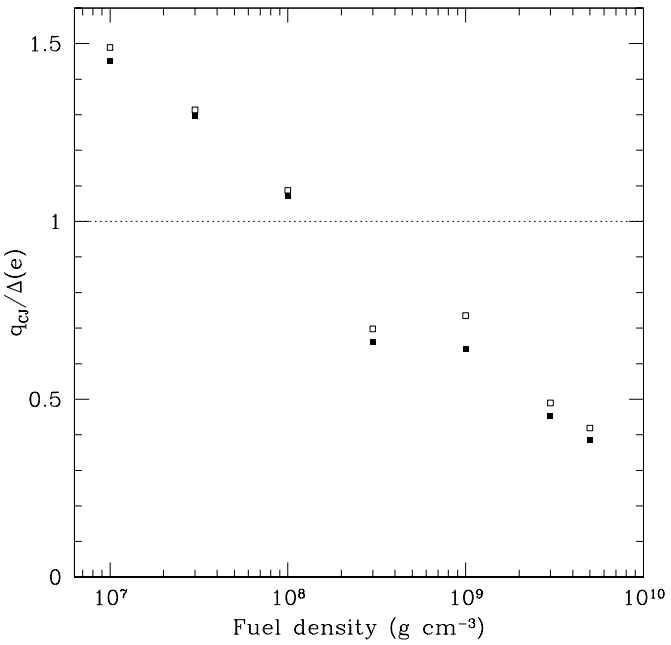

Fig. 3. Ratio of the nuclear energy released in a Chapman-Jouguet detonation, q_{CJ}, to the increase in specific internal energy of the fuel needed to achieve the shocked state, $\Delta(e)$, as a function of fuel density. Open squares belong to a fuel composition of $X(^{12}C) = X(^{16}O) = 0.5$, while solid squares are for initial composition $X(^{12}C) = 0.2$ and $X(^{16}O) = 0.8$. A dotted line indicates the minimum q_{CJ} necessary for self-sustained detonation propagation $q_{CJ} = \Delta(e)$.

the flame reaches the mantle before the detonation initiation has succeeded and finally fails to burn the WD.

4.3. Parametric dependencies

We examine here what variations, if any, are introduced by changing the initial setup of the explosion models.

4.3.1. Composition of the mantle

Models 9 and 16 are similar to models 7 and 15 (pure detonations of $M_{CO} = 0.3$ and $0.4\ M_\odot$), respectively, but the former models have a higher ^{16}O abundance in the ONe mantle. The change of the composition of the mantle has no effect on the explosion of the model with the smaller M_{CO}. However, the detonation of the $M_{CO} = 0.4\ M_\odot$ case is completely different. With the larger ^{16}O abundance, the piston formed by the detonated carbon-rich region is energetic enough to allow the incineration of almost the whole WD. This shows how a moderate change in the initial conditions can have a huge impact on the final outcome of the explosion of these structures, and that the $M_{CO} = 0.4\ M_\odot$ case is on the frontier between those that leave a massive bound remnant and those that produce an ejecta that is very rich in ^{56}Ni.

In models 2 and 8, we explored the effect that a small residual abundance of ^{12}C in the ONe mantle has on DETO models with $M_{CO} = 0.2$ and $0.3\ M_\odot$ cases (to be compared to models 1 and 7). For the smaller M_{CO}, there is no change at all. For the $0.3\ M_\odot$ case, the only change is that the detonation penetrates slightly more in the ONe mantle. Although it is not enough to make a healthy explosion, the ejecta mass is larger at $0.49\ M_\odot$ instead of $0.37\ M_\odot$. As the ejecta is in any case devoid of radioactive isotopes, this change is not expected to have any observational consequences.

4.3.2. Structure of the accreted mantle

More complex structures of the mantle have been explored in models 3, 6, 17, and 18, which have a thick carbon-rich layer surrounding the ONe shell. The results, which have to be compared to models 1, 5, and 15, show no significant impact of the presence of such chemically differentiated mantles, apart from slight differences in the remnant mass in the case of a DDT explosion.

4.3.3. Mixing during carbon simmering

Convective mixing during carbon simmering is a potential source of homogenization of the WD composition prior to explosion. Assuming full chemical mixing of the initial WD models with $M_{CO} = 0.2$, 0.3, and $0.4\ M_\odot$ and default mantle composition, i.e., without carbon, the global ^{12}C mass fractions are $X(^{12}C) = 0.05$, 0.07, and 0.09, respectively. Contrary to the results of chemically differentiated hybrid cores described in previous sections, the composition and structure of the mantle may have an influence on the outcome of fully mixed models. This effect is particularly relevant if the mantle is composed of two layers, of which one is rich in carbon, as is assumed in some of the models in Table 1 and Sect. 4.3.2. For instance, assuming full chemical mixing of the initial WD models with $M_{CO} = 0.2$, 0.3, and $0.4\ M_\odot$, a middle layer with no carbon and an external layer of $M_{ext} = 0.57\ M_\odot$ with $X_{ext}(^{12}C) = 0.32$, the global ^{12}C mass fractions are $X(^{12}C) = 0.18$, 0.20, and 0.23, respectively. We computed the explosion (DETO and DDT modes) of two models representative of the class of homogenized MSHC models, one in which $X(^{12}C) = 0.10$ and the other with $X(^{12}C) = 0.20$ (models 24–27 in Table 1).

Pure detonation of these homogeneous models (24 and 26) are similar to the successful[5] pure detonations of hybrid cores with M_{CO} from 0.4 to $0.74\ M_\odot$. They are able to propagate across most of the WD, unbinding the whole star and ejecting a huge mass of ^{56}Ni. The impact of mixing on the result of pure detonations is, thus, to eliminate the diversity on the outcomes, in particular, the possibility that the explosion leaves a massive bound remnant.

The delayed detonation of the homogeneous model with $X(^{12}C) = 0.10$ (model 25) is not able to unbind the WD completely. The small mass fraction of ^{12}C makes the release of nuclear energy too small to initiate a healthy detonation, and the burning front dies after having consumed $\sim 0.35\ M_\odot$. The final result is rather similar to that of the pure detonation of the hybrid-core case with $M_{CO} = 0.2\ M_\odot$.

The delayed detonation of the homogeneous model with $X(^{12}C) = 0.20$ (model 27) leads to outcomes similar to those obtained from the hybrid core cases with the same ρ_{DDT} and $M_{CO} > 0.2\ M_\odot$.

We also computed the explosion (DDT model 28) of a homogeneous model with chemical composition obtained from the full mixing of the hybrid core model 23 (middle panel in Fig. 1). In this case, the global carbon mass fraction is $X(^{12}C) = 0.28$, which is very close to the value of the carbon mass fraction in the carbon-rich core of model 23. Indeed, the outcome of the delayed detonation of both models reported in Table 1 is within 2–3% of each other. All in all, successful delayed detonations of homogeneous models seem to encompass a narrower range of ejecta properties than their hybrid-core counterparts.

[5] Here, by successful we mean that the detonation progressed through a substantial fraction of the WD, as in models 16, 20, and 22, whereas in models 15, 17, and 18 half of the WD mantle remained with its original composition.

We conclude that the main effect of the eventual destruction of the chemically differentiated structure (hybrid core) during the carbon simmering phase is a reduction in the variation of the possible outcomes, but they do not qualitatively affect the properties of successful explosions.

4.3.4. Comparison to Kromer et al. (2015)

The initial model in Kromer et al. (2015) was a cold, chemically differentiated, WD with a central density of 2.9×10^9 g cm^{-3}. Their chemical structure consisted of a carbon-rich, $X(^{12}\mathrm{C}) = 0.5$, core of $M_{\mathrm{CO}} = 0.2\ M_\odot$ surrounded by an ONe layer of $0.9\ M_\odot$ (with a 3% carbon abundance by mass) and topped by a CO layer of $0.3\ M_\odot$. This initial model is most similar to those of our models 1–6.

The main difference between our calculations and those of Kromer et al. (2015) lies on the assumed geometrical configuration of the flame at runaway, a major unknown in theoretical studies of SNIa explosion. While our simulations necessarily start, owing to the one-dimensional nature of our code, from a spherically symmetric volume at the center of the WD, they ignite five kernels off-center. These kernels soon merge, forming a one-sided plume that floats toward the surface while the flame grows in size. Finally, in the simulation of Kromer et al. (2015) less than half the CO core is consumed by the deflagration, and only $0.014\ M_\odot$ of material is ejected of which $3.4 \times 10^{-3}\ M_\odot$ are ^{56}Ni.

Unlike the model of Kromer et al. (2015), in all of our explosion models 1–6 the whole CO core is consumed by the burning front. Their final results are intermediate between those of our models 1–3 and 4–6. In the first group, there is left a massive remnant, as in Kromer et al. (2015) model, but no ^{56}Ni is ejected. In the second group, there is a small amount of ^{56}Ni ejected, but at a very low velocity because of the large mass of the ejecta. We speculate that because the initial geometry of the flame may not be always the same, it is possible that all of these models are realized in nature.

5. Discussion

The ultimate verification of a supernova model relies on the comparison of synthetic spectra and light curves with observations. However, our purpose is to identify the most promising models for future computation of their optical properties. To this aim, we base the following discussion on the location of the computed models in the kinetic energy vs ejected ^{56}Ni mass plane (Fig. 2) and in the chemical profile as a function of velocity (Fig. 4).

In Fig. 2 we plot our reference models 29–32 (open triangles) together with the models computed by Ohlmann et al. (2014), who explored the delayed detonation of Chandrasekhar-mass WDs with homogeneous composition and variable abundance of ^{12}C, 0.2–0.5 in mass fraction (crosses). These models (labeled "A" in the plot) help identify the combination of kinetic energy and ejected mass of ^{56}Ni necessary to obtain a normal SNIa, $K \simeq 1.0\text{–}1.5 \times 10^{51}$ erg and 0.3–0.8 $M_\odot$ of ^{56}Ni (Mazzali et al. 2007; Woosley et al. 2007). The range of ^{56}Ni masses can be extended down to $0.08\ M_\odot$ and up to $0.94\ M_\odot$ to account for the full set of SNIa that follow the light-curve, luminosity-width relation (dashed line) (Mazzali et al. 2007).

Pure detonation models that burn the ONe mantle (models 16, 20, 22, 24, and 26 in Table 1, or "B" in the plot) lie to the right of the normal SNIa models with similar kinetic energy but much larger $M(^{56}\mathrm{Ni})$. These models burn almost all of the WD at high density, so they synthesize at most a few thousandths of a solar mass of IME, which is in clear contradiction with the requirement of prominent Si and S absorption features that define SNIa (aside from the absence of hydrogen). Such an object has never been observed. On the other hand, pure detonations that did not succeed in burning a significant fraction of the ONe mantle leave a huge remnant and eject from a few hundredths to a few tenths of a solar mass of material with the original composition of the mantle, i.e., with no radioactive isotopes. These explosions would not be detectable as a supernova and are labeled "no optical display" in Table 1. Their remnants would expand as a result of the large energy content and radioactive input of the supernova, and would remain brighter-than-normal ONe WDs during a Kelvin-Helmholtz timescale.

Region "C" in Fig. 2 is populated by delayed detonations of hybrid-core WD with carbon-rich central volumes of $0.3\ M_\odot$ or more, either chemically differentiated (models 10–14, 19, 21, 23) or homogeneous (models 27 and 28) at thermal runaway. This group of models is characterized by slightly smaller amounts of ^{56}Ni ejected and substantially smaller kinetic energies than normal SNIa models. Both tendencies point toward the subluminous class of SNIax. White et al. (2015) distinguishes two different populations within the SNIax class. One population, which they call SN2002es-like, is characterized by small dispersion of light-curve properties with rise times slightly faster than normal SNIa, slow ejecta, and a preference for early-type host galaxies. Their ejecta mass is thought to be of order $\sim 0.5\ M_\odot$. The other population, which they call after SN2002cx, presents a larger dispersion of light-curve shapes, but the rise times are consistently slower than in normal SNIa, the ejecta speed is slightly faster than in the SN2002es-like population, and they are usually hosted by late-type galaxies. Their ejecta mass can be as large as the Chandrasekhar mass, depending on the effective opacity assumed by White et al. (2015; also see McCully et al. 2014b).

The velocity distribution of the explosion products in some delayed detonation models located in region "C" is shown in Fig. 4, together with the result of the reference delayed detonation model 30. Panel (a) shows the velocity distribution for the LHC DDT model 23. Comparing with the bottom panel, (d), it is clear that the LHC models are distinguished by Si and S extending up to much lower velocities than in the reference model[6]. For instance, $X(\mathrm{Si}) \geq 0.1$ below $\sim$24 000 km s^{-1} in the reference model, while the limit is $\sim$16 000 km s^{-1} in the uppermost panel, i.e., $\sim$8000 km s^{-1} slower. On the other hand, the tip of the ^{56}Ni-rich core is $\sim$2000 km s^{-1} slower in the hybrid-core model than in the reference model. The relatively short distance between the radioactive core and the Si-rich region might explain the hotter than normal photospheres deduced for the SNIax class.

Panels b and c of Fig. 4 show the chemical structure of delayed detonations of both chemically differentiated and homogeneous models coming from $M_{\mathrm{CO}} = 0.3\ M_\odot$, MSHC models 12 and 27. The structure of the ^{56}Ni-rich inner ejecta is very similar to the other models shown in the same plot, and yet Si and S extend to much smaller velocities, so they are even closer to the radioactive core than they are in the LHC models. This trend is suggestive of a correlation between dimmer objects and hotter

[6] In this comparison, we disregard the effects due to the inclusion of solar metallicity abundances in the pre-explosive structure of the reference model, which leaves an imprint in the ^{56}Ni-rich core in the form of large Mn and Ni abundances, and in the outermost layers as the presence of iron.

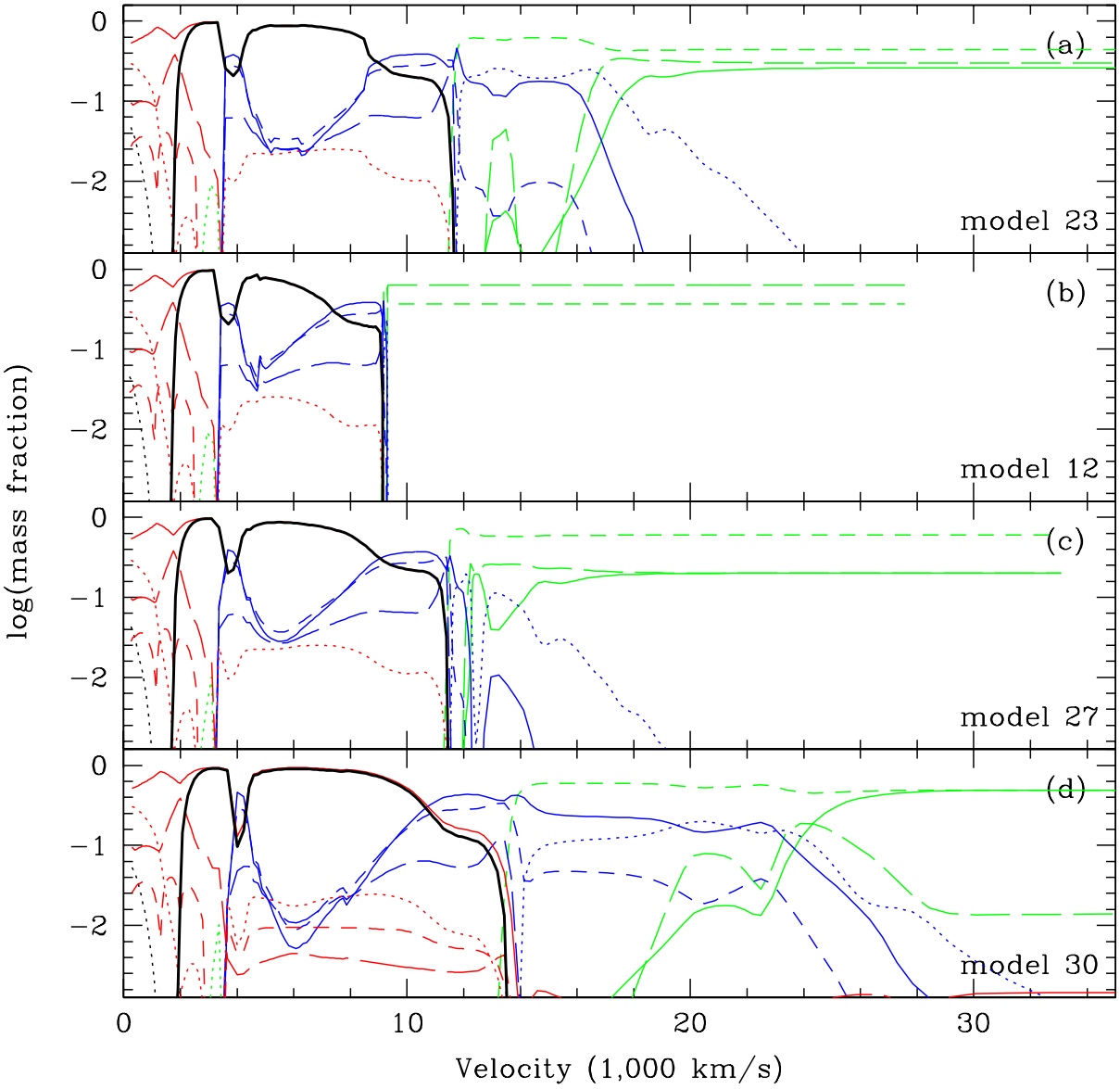

Fig. 4. Chemical composition of the ejected matter in four delayed detonation models with $\rho_{\rm DDT} = 1.4 \times 10^7$ g cm^{-3}. *From top to bottom*: hybrid WD with a $M_{\rm CO} = 0.74\ M_\odot$ (model 23); hybrid WD with $M_{\rm CO} = 0.3\ M_\odot$ (model 12); mixed model with an initial $X(^{12}{\rm C}) = 0.20$ (model 27); and pure CO WD with an initial homogeneous composition with $X(^{12}{\rm C}) = X(^{16}{\rm O}) \simeq 0.5$ and solar mass fractions of species with $A \geq 24$ (model 30). The black thick line is the abundance by mass of ^{56}Ni a few seconds after explosion. The rest of lines give the abundance by mass of the most important elements after radioactive decays (i.e., the final stable isotopes), and have the following meaning: green stands for fuel (solid is C, short dashed is O, and long dashed is Ne); blue stands for IME (solid is Si, dotted is Mg, short dashed is S, and long dashed is Ca); and red stands for IGE (solid is Fe, dotted is Cr, short dashed is Mn, and long dashed is Ni).

photospheres, but such a correlation has not yet been reported for SN2002cx-like objects.

The SNIax group extend to very low luminosities that require less than a hundredth of a solar mass of ^{56}Ni ejected, e.g., SN2008ha or SN2007qd. Models labeled as "slow ejecta" in Table 1 (models 4–6, 15, 17, and 18, "D" in Fig. 2[7]) produce and eject similar amounts of ^{56}Ni. They are able, as well, to account for the small specific kinetic energy of the ejecta required to explain these supernovae. However, the ejecta mass in the models is close to the Chandrasekhar mass, while these events are usually explained as low-mass ejecta (McCully et al. 2014b; White et al. 2015). Since the energy released in these models is close to the bounding energy of the progenitor WD, we cannot discard that some multidimensional hydrodynamics effect can redistribute the kinetic energy in such a way that a larger remnant is left. Interestingly, Kromer et al. (2015) show that an asymmetrical pure deflagration of a hybrid-core, Chandrasekhar-mass WD can match the observational properties of SN2008ha, one of the faintest SNIax ever recorded, although the ejected mass seems to be too small to account for this particular supernova. Nevertheless, the model was not specially tuned to reproduce the observables of SN2008ha, and the parameter space was not explored to find a better agreement. So, it is likely that relatively small differences in the initial model can result in a better fit of the properties of SN2008ha.

With respect to the other aforementioned subclasses of subluminous SNIa, both the .Ia and the Ca-rich subclasses are not

[7] Note that models 15, 17, and 18 cannot be distinguished in this fig. because their location coincides with that of DDT model 6.

compatible with any of the models we calculated. The .Ia class is characterized by a very fast rise of the light curve, which is at odds with the large mass of the ejecta we obtain (unless there is some multidimensional hydrodynamics effect, as mentioned in the previous paragraph). On the other side, we do not see any model that is particularly rich in calcium, as observed in the Ca-rich group.

6. Conclusions

We have contributed to the study of the impact of hybrid-core WDs on the understanding of SNIa and their diversity. We calculated the explosion of Chandrasekhar-mass, hybrid-core WDs, with different masses of the carbon-rich central volume. We aim to identify the combination of evolutionary scenario and explosion mechanism that provide potential models for peculiar SNIa and whose light curve and spectra should be addressed in future works.

Pure detonations of Chandrasekhar-mass CO WDs have been dismissed for decades as possible mechanisms of SNIa explosion because they turn almost the whole star into IGE ashes. However, the presence of an ONe mantle in hybrid-core WDs opened the possibility that pure detonations succeed in producing enough intermediate-mass elements to match the observational properties of, at least, some subgroup of SNIa. Our results show that this is not the case. Indeed, the presence of an ONe mantle may have a strong impact on the propagation of a detonation, but the outcome is different from any kind of thermonuclear supernova observed so far. If the carbon-rich region is too small, $M_{\rm CO} \lesssim 0.3\ M_\odot$, the detonation dies shortly after entering the ONe mantle with the result that the nuclear energy release is too small and most of the WD remains bound after the thermonuclear event. A few tenths of a solar mass can be ejected, but are devoid of radioactive elements. As a result, nothing like a supernova is to be expected. On the other hand, if the carbon-rich region is large enough that the propagation of the detonation through the ONe mantle can be sustained by the piston action of the incinerated core, then almost the whole WD is burned to ashes. In such a case, as in the pure CO composition case, the ejecta would contain no IMEs in contradiction with SNIa observations. The same result is obtained if the chemical composition is mixed just before thermal runaway, during the carbon simmering phase, even for small masses of the carbon-rich central volume. We conclude that pure detonations in hybrid-core WDs can be discarded as the explosion mechanism behind any known class of SNIa, just as for pure CO WDs.

But, if the explosion mechanism is of the delayed detonation kind, the properties of the ejecta from hybrid-core WDs are reminiscent of the subluminous class SNIax, in particular, the SN2002cx-like population (White et al. 2015). They are characterized by slower velocities than our reference models for normal SNIa and by a smaller extent of the Si and S-rich layers that are closer to the ^{56}Ni-rich core. We suggest that the proximity of the IMEs to the radioactive sources may explain the hot photospheres often detected in SNIax, which would imply an inverse correlation between photosphere temperature and supernova luminosity. Our simulations of delayed detonations of hybrid-core WDs are scarcely sensitive to the mixing of the chemical composition during the carbon simmering phase. Another appealing feature of hybrid-core WDs as SNIax progenitors is that they come from stars more massive than CO WDs and the secondary must be heavier than 3–4 $M_\odot$ (see Sect. 2), which may explain the preference of SN2002cx-like objects for galaxies with active stellar formation regions in a natural way.

On the other hand, our models do not cover the whole range of ^{56}Ni ejected masses that seems to be implied by current observations of SNIax. Specifically, we do not find models that leave a massive remnant and eject a ^{56}Ni mass as small as 0.1 $M_\odot$ or less (the smallest amount of ^{56}Ni in our models is 0.27 $M_\odot$, but its precise value depends on the assumed $\rho_{\rm DDT}$). This could be related to the limitations implicit in our one-dimensional study of the explosion of hybrid-core WDs. For instance, our delayed-detonation explosions of carbon-rich central volumes of 0.2 $M_\odot$ eject a few hundredths of a solar mass of ^{56}Ni, but the whole ejecta mass is too large for the imparted kinetic energy. In this case, the expected light curve would be much wider than observed. In an asymmetrical event, some bullets of ^{56}Ni-rich matter could float through the ONe mantle during the deflagration phase of the explosion, redistributing the energy in such a way that the ejecta mass were smaller (Bravo & García-Senz 2006; Bravo & García-Senz 2009), i.e., closer to that needed to explain the dimmest SNIax.

The explosions we calculated are restricted to Chandrasekhar-mass WDs, which could arise either from the SD or the DD (slow merger) scenario. However, hybrid-core WDs may experience a thermonuclear explosion in other scenarios, such as double-detonations of sub-Chandrasekhar-mass WDs, explosions of Chandrasekhar-mass WDs surrounded by low-density haloes (coming from a DD merger), violent mergers, and violent collisions, several of which require multidimensional simulations. We will explore such problems in future works.

Acknowledgements. We thank the referee for useful suggestions that have improved the presentation. This work was supported by Spanish MINECO grants AYA2012-33938 and AYA2013-40545.

References

Badenes, C., Bravo, E., Borkowski, K. J., & Domínguez, I. 2003, ApJ, 593, 358
Bravo, E., & García-Senz, D. 2006, ApJ, 642, L157
Bravo, E., & García-Senz, D. 2009, ApJ, 695, 1244
Bravo, E., & Martínez-Pinedo, G. 2012, Phys. Rev. C, 85, 055805
Burrows, A. 2013, Rev. Mod. Phys., 85, 245
Campbell, S. W., & Lattanzio, J. C. 2008, A&A, 490, 769
Chen, M. C., Herwig, F., Denissenkov, P. A., & Paxton, B. 2014, MNRAS, 440, 1274
Denissenkov, P. A., Herwig, F., Truran, J. W., & Paxton, B. 2013, ApJ, 772, 37
Denissenkov, P. A., Truran, J. W., Herwig, F., et al. 2015, MNRAS, 447, 2696
Doherty, C. L., Siess, L., Lattanzio, J. C., & Gil-Pons, P. 2010, MNRAS, 401, 1453
Doherty, C. L., Gil-Pons, P., Siess, L., Lattanzio, J. C., & Lau, H. H. B. 2015, MNRAS, 446, 2599
Dominguez, I., Tornambe, A., & Isern, J. 1993, ApJ, 419, 268
Drout, M. R., Soderberg, A. M., Mazzali, P. A., et al. 2013, ApJ, 774, 58
Eldridge, J. J., & Tout, C. A. 2004, MNRAS, 353, 87
Farmer, R., Fields, C. E., & Timmes, F. X. 2015, ApJ, 807, 184
Foley, R. J., Challis, P. J., Chornock, R., et al. 2013, ApJ, 767, 57
Foley, R. J., McCully, C., Jha, S. W., et al. 2014, ApJ, 792, 29
Frost, C. A., & Lattanzio, J. C. 1996, ApJ, 473, 383
Garcia-Berro, E., & Iben, I. 1994, ApJ, 434, 306
Gil-Pons, P., & García-Berro, E. 2001, A&A, 375, 87
Gil-Pons, P., García-Berro, E., José, J., Hernanz, M., & Truran, J. W. 2003, A&A, 407, 1021
Gil-Pons, P., Doherty, C. L., Lau, H., et al. 2013, A&A, 557, A106
Grevesse, N., & Noels, A. 1993, in Origin and Evolution of the Elements, eds. N. Prantzos, E. Vangioni-Flam, & M. Casse (Cambridge University Press), 15
Gutiérrez, J., Garcia-Berro, E., Iben, Jr., I., et al. 1996, ApJ, 459, 701
Gutiérrez, J., Canal, R., & García-Berro, E. 2005, A&A, 435, 231
Howell, D. A. 2011, Nat. Comm., 2, 350
Ibeling, D., & Heger, A. 2013, ApJ, 765, L43
Janka, H.-T., Langanke, K., Marek, A., Martínez-Pinedo, G., & Müller, B. 2007, Phys. Rep., 442, 38

Janka, H.-T., Hanke, F., Hüdepohl, L., et al. 2012, Prog. Theor. Exp. Phys., 2012, 01A309
Kasliwal, M. M., Kulkarni, S. R., Gal-Yam, A., et al. 2010, ApJ, 723, L98
Kasliwal, M. M., Kulkarni, S. R., Gal-Yam, A., et al. 2012, ApJ, 755, 161
Khokhlov, A. M. 1988, Ap&SS, 149, 91
Kromer, M., Ohlmann, S. T., Pakmor, R., et al. 2015, MNRAS, 450, 3045
Li, W., Filippenko, A. V., Chornock, R., et al. 2003, PASP, 115, 453
Mazzali, P. A., Röpke, F. K., Benetti, S., & Hillebrandt, W. 2007, Science, 315, 825
McCully, C., Jha, S. W., Foley, R. J., et al. 2014a, Nature, 512, 54
McCully, C., Jha, S. W., Foley, R. J., et al. 2014b, ApJ, 786, 134
Meng, X., & Podsiadlowski, P. 2014, ApJ, 789, L45
Miyaji, S., Nomoto, K., Yokoi, K., & Sugimoto, D. 1980, PASJ, 32, 303
Moll, R., Raskin, C., Kasen, D., & Woosley, S. E. 2014, ApJ, 785, 105
Nomoto, K. 1984, ApJ, 277, 791
Nomoto, K. 1987, ApJ, 322, 206
Nomoto, K., Saio, H., Kato, M., & Hachisu, I. 2007, ApJ, 663, 1269
Ohlmann, S. T., Kromer, M., Fink, M., et al. 2014, A&A, 572, A57
Pakmor, R., Kromer, M., Röpke, F. K., et al. 2010, Nature, 463, 61
Parrent, J., Friesen, B., & Parthasarathy, M. 2014, Ap&SS, 351, 1
Parthasarathy, M., Branch, D., Jeffery, D. J., & Baron, E. 2007, New Astron. Rev., 51, 524
Perets, H. B., Gal-Yam, A., Mazzali, P. A., et al. 2010, Nature, 465, 322
Piro, A. L., & Bildsten, L. 2008, ApJ, 673, 1009
Piro, A. L., & Chang, P. 2008, ApJ, 678, 1158
Podsiadlowski, P., Mazzali, P., Lesaffre, P., Han, Z., & Förster, F. 2008, New Astron. Rev., 52, 381
Raskin, C., Kasen, D., Moll, R., Schwab, J., & Woosley, S. 2014, ApJ, 788, 75
Ritossa, C., García-Berro, E., & Iben, Jr., I. 1999, ApJ, 515, 381
Saio, H., & Nomoto, K. 1998, ApJ, 500, 388
Shingles, L. J., Doherty, C. L., Karakas, A. I., et al. 2015, MNRAS, 452, 2804
Siess, L. 2006, A&A, 448, 717
Siess, L. 2010, A&A, 512, A10
Smartt, S. J. 2009, ARA&A, 47, 63
Stein, J., & Wheeler, J. C. 2006, ApJ, 643, 1190
Stritzinger, M. D., Valenti, S., Hoeflich, P., et al. 2015, A&A, 573, A2
Valenti, S., Yuan, F., Taubenberger, S., et al. 2014, MNRAS, 437, 1519
Ventura, P., & D'Antona, F. 2011, MNRAS, 410, 2760
Waldman, R., & Barkat, Z. 2007, ApJ, 665, 1235
White, C. J., Kasliwal, M. M., Nugent, P. E., et al. 2015, ApJ, 799, 52
Woosley, S., & Janka, T. 2005, Nat. Phys., 1, 147
Woosley, S. E., Heger, A., & Weaver, T. A. 2002, Rev. Mod. Phys., 74, 1015
Woosley, S. E., Kasen, D., Blinnikov, S., & Sorokina, E. 2007, ApJ, 662, 487